ColHySE: An Advanced Column Hydrodynamic-based model for Solvent Extraction

Sophie Charton, Simone Castellano, Samer Alzyod, Nida Sheibat-Othman

ColHySE: An Advanced Column Hydrodynamic-based model for Solvent Extraction

Sophie Charton[1]*, Simone Castellano[1,2], Samer Alzyod[1], Nida Sheibat-Othman[2]

[1] CEA, DES, ISEC, DMRC, Univ. Montpellier, Marcoule, France

[2] University of Lyon, Université Claude Bernard Lyon 1, CNRS, UMR 5007, LAGEPP, Villeurbanne, France

* *Corresponding author:* sophie.charton@cea.fr

Abstract:

An original one dimensional population balance model (PBM)-based model of liquid-liquid extraction columns is reported. Compared to existing simulators, *ColHySE* implements a more realistic description of the flow patterns in the contactor, and predicts its effect on the local droplet-droplet interactions (*i.e.* breakage and coalescence rates). Proper turbulent properties, extracted from single-phase flow CFD simulations, are used in the source terms of the PBM to evaluate locally the inhomogeneous breakage and coalescence rates, using the *averaged* Coulaloglou and Tavlarides kernels (Castellano *et al.*, 2018). The sensitivity of the predicted droplets mean diameter, $d_{32,}$ and the holdup, ϕ, to the parameters of the used empirical and phenomenological models, on the one hand, and to the operating conditions of the column, on the other hand, was studied. Although some model parts must be refined, and an experimental validation remains necessary, the results confirm that the 1D-PBM methodology used in ColHySE is relevant for predicting the interfacial area in the pulsed column as a function of the operating conditions and geometry, hence highlighting its relevance to study the hydrodynamic stability and tendency to flooding. The sensitivity analysis has moreover highlighted the needs for an improved slip velocity model.

Keywords:

Solvent extraction column, two-phase flow, population balance equation, averaged kernels, advanced hydrodynamics description.

1 Introduction

Various types of contactors can be used to implement solvent extractions: extraction columns, mixer-settlers and centrifugal contactors. In the case of columns, where the two liquid phases flow counter-currently, the extraction proceeds continuously along the axial direction. Agitated columns, as Rotating Discs Columns (*e.g.* Kühni or Batman) exhibit a relative flexibility towards the solvent properties or the feed concentration, and are preferred in hydrometallurgy, whereas pulsed column, packed with discs and doughnuts (DD) or with perforated plates internals, remain the most preferred contactors in nuclear applications, due to their robustness and low maintenance requirements (J. C. Godfrey and Slater, 1994). The typical geometries and operating conditions of these different contactors strongly influence the concentration of interface area between the two liquid phases and hence affect the extraction efficiency. While a large interfacial area favors the extraction, reducing too much the size of the droplets can lead to flooding and other stability and phase separation or phase entrainment issues, which are highly detrimental to the column performances. It is hence of great interest for process design, optimization purposes, and the selection of the appropriate technology for a given liquid-liquid extraction problem, to be able to predict the interfacial area and its evolutions across scales. In pulsed columns, the interfacial area between the two non-miscible liquids results from the joint effects of the packing geometry (*e.g.* the free area and the spacing between the packing elements) and the pulsation intensity.

Accurate prediction of the drop size distribution (DSD) and the dispersed phase volume fraction in the column (or the holdup, ϕ), as a function of its geometry and operating conditions is hence required. Empirical correlations are available in the literature to estimate

these properties (Boyadzhiev and Spassov, 1982; Kumar and Hartland, 1996; Pacek, Man and Nienow, 2005) but they are only valid within the range of operating conditions in which they were established, and their extrapolation is hazardous. Better predictions can be obtained by implementing a Population Balance Equation model (PBE) that requires the computation of the droplet breakage and coalescence rates used as source terms. Since the prior work of Casamatta (Casamatta, 1981), many works have been devoted to the modeling of liquid-liquid extraction columns using PBE, either based on class method (Al Khani, Gourdon and Casamatta, 1989; Attarakih, Alzyod and Fricke, 2017), or on the method of moments (Attarakih *et al.*, 2015). In each case, the column is considered as a 1D axial domain along which the PBE is solved, and in most of them, if not all, the turbulent breakage and coalescence kernels are based on the inertial subrange of the Kolmogorov theory (Batchelor, 1982), and are only dependent on the turbulent kinetic energy dissipation rate ε. They moreover suppose uniform source terms, which means that a uniform turbulent dissipation rate is assumed to prevail in the column. It is however well known that ε is far from being uniform in most liquid-liquid contactors and that this assumption, despite the obvious simplification it brings, can lead to significant uncertainties in the performance predictions across scales. It is now generally accepted that a significant improvement in the predictive character of solvent extraction models cannot be obtained without a better description of the flow in the apparatus, and of its couplings with the population of droplets. A large number of fluid dynamic studies have therefore been dedicated in recent years to the simulation of flows in extraction columns. Similarly, thanks to increasing numerical resources, coupled CFD-PBE simulations are becoming more easily applicable. The latter are usually performed using a RANS approach, which is particularly convenient when dealing with droplets breakage and coalescence, as it directly gives the turbulent dissipation rate. In these coupled approaches, the CFD code, usually ANSYS- FLUENT(Amokrane *et*

al., 2016) or OpenFOAM (Li *et al.*, 2017), provides the local flow field variables and the energy dissipation rate, while the PBE is solved in each cell of the computational domain.

In a previous study, (Amokrane *et al.*, 2016) predicted the discrete phase holdup and droplet mean diameter in a 25 mm inner diameter DD column. They solved the PBE using the Quadrature Method Of Moments (QMOM) algorithm (Marchisio, Vigil and Fox, 2003), considering the Coulaloglou and Tavlarides kernels as source terms (Coulaloglou and Tavlarides, 1977). The four kernels parameters had been identified beforehand using a first series with in situ DSD and hold-up measurements. More recently, (Alzyod, Attarakih and Bart, 2018) developed a coupled CFD-PBE model to predict the extraction performances of pulsed sieve plate columns, *i.e.* including the mass transfer problem. As in (Amokrane *et al.*, 2016), the breakage and coalescence model parameters had to be evaluated in advance, in this case by simulations. While being promising, CFD-PBE simulations require heavy multicore equipment and are therefore not suitable for simulating an entire extraction column. Advanced modeling approaches in chemical engineering are still needed to predict the sensitivity of extraction columns functioning towards geometrical and operating parameters (Hlawitschka *et al.*, 2016). This is the aim of the original model *ColHySE* introduced in this work.

Previous work dedicated to emulsification in closed stirred tanks (Castellano *et al.*, 2018) demonstrated that the Sauter mean diameter of the dispersed phase, and its evolution with the stirring rate, and nature of the dispersed phase, can be efficiently predicted by a 0D simulation. Indeed, using the steady-state probability density function $f(\varepsilon)$ of the turbulent dissipation rate in the closed vessel, the prediction of the mean diameter can be conveniently decoupled from the 3D hydrodynamic description of the contactor. This methodology, based on the computation of *volume-averaged* coalescence and breakage kernels has enabled to identify a set of empirical parameters which, although not universal, are more robust to

changes in the flow properties. It is here extended to the case of a 1D contactor, where *i)* the flow is periodically varying with time, and *ii)* along which the dispersed phase properties and holdup are not uniform, nor constant over time. By this way, relation with fluid dynamic simulation results is ensured but in a simplified 1-D hydrodynamic model, which ensures faster computation, while accounting for the main turbulence effects on the dispersed phase properties to be predicted, without systematic adjustment of the parameters.

The study is hydrodynamic only, *i.e.* considers the evolution of the size of droplets and the holdup, but not mass transfer. It is based on the 25 mm inner diameter pulsed liquid-liquid extraction column for which some experimental values of holdup and Sauter mean diameter have already been published (Amokrane *et al.*, 2016). The founding principles and the structure of the model are described in Sec. 2, giving the details of the equations solved in the 1D domain. In Sec. 3, we discuss the impact of the time-step used when averaging the *pdf(*ε*)* in the periodical pulsed flow. An analysis of the sensitivity of the predicted interfacial area to the adjustable parameters of the closure models, including the 4 parameters of the breakage and coalescence kernels, is also given. The aim is to highlight the weight of the different interactions between the phases and to point out which closure models require special attention or additional developments. At last in Sec. 4, we perform a sensitivity analysis of the dispersed phase properties to the column operating parameters, to highlight the great flexibility of the proposed advanced hydrodynamic description for the prediction of the interfacial area, which is of prime importance for solvent extraction operations.

2 Model description

The methodology that had been considered in the case of a closed stirred tank reactor (at 0D level) in our previous work (Castellano *et al.*, 2018) is here extended along the spatial domain to model the hydrodynamic behavior of a solvent extraction column (Fig. 1). There are two main differences in the implementation of the PBE using averaged kernels in the

pulsed column simulator compared to the stirred tank. First, the droplet properties, assumed to be uniformed in the stirred-tank, are likely to evolve in the axial direction in the case of the column, while they are transported by the flow. Secondly, the flow dynamic is much slower in the periodically oscillating flow that prevails in the column, meaning that the time-averaging of the breakage and coalescence kernels has also to be considered.

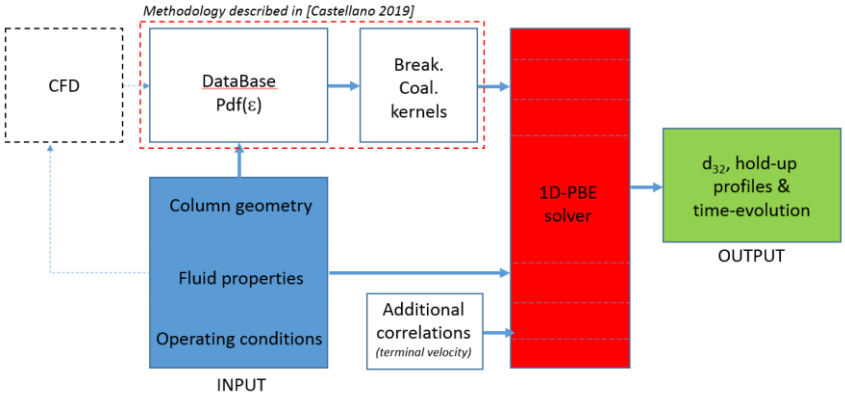

Figure 1: Schematic representation of the model structure

2.1 General formulation of the 1D axial – PBE model

The PBE model is used to describe the evolution of the droplet size in time and along the column. In the most general 3D case, the PBE considers a number density function which is function of the internal coordinates $\boldsymbol{\varphi}$, the spatial coordinates $\boldsymbol{x}$ ($\boldsymbol{x} = [x, y, z]$) and the time t (Ramkrishna, 2000; Marchisio and Fox, 2013). As we are interested in tracking the interfacial area and the dispersed phase volume fraction, only the droplet volume v will be considered as internal coordinate ($\boldsymbol{\varphi} = v$). Therefore, the 3D PBE reduces to:

$$\frac{\partial}{\partial t} n(v, \boldsymbol{x}, t) + u(v, \boldsymbol{x}, t) \frac{\partial}{\partial \boldsymbol{x}_i} n(v, \boldsymbol{x}, t) = S(v, \boldsymbol{x}, t) \tag{1}$$

Where $\boldsymbol{x}_i$ represents the coordinates of section i of the column, $n(v, \boldsymbol{x}, t)$ is the number density of droplets per unit volume of the column, and the source term $S(v, \boldsymbol{x}, t)$ stands for:

$$S(v,\boldsymbol{x},t)=\int_{v}^{\infty}\beta(v|v')\Gamma(v',\boldsymbol{x})n(v',\boldsymbol{x},t)\mathrm{d}v'-\Gamma(v,\boldsymbol{x})n(v,\boldsymbol{x},t)$$

$$+\frac{1}{2}\int_{0}^{v}Q(v-v',v',\boldsymbol{x},)\,n(v-v',\boldsymbol{x},t)n(v',\boldsymbol{x},t)\mathrm{d}v' \qquad (2)$$

$$-n(v,\boldsymbol{x},t)\int_{0}^{\infty}Q(v,v',\boldsymbol{x})n(v',\boldsymbol{x},t)\,\mathrm{d}v'$$

Γ and Q are the breakage and coalescence kernels and $\beta(v|v')$ is the daughter distribution function.

To adapt to the 1D formalism chosen for extraction columns, the PBE model can be simplified assuming a number density function dependent only on one spatial coordinate (*i.e.* the axial coordinate z) while being homogeneous in the column section, with Ω the cross sectional area:

$$\bar{n}(v,z,t)=\frac{1}{\Omega}\int_{\Omega}n(v,\boldsymbol{x},t)\mathrm{d}\Omega \qquad (3)$$

Despite this assumption, the PBE model remains 3D-space dependent, due to the breakage and coalescence kernels. Therefore, the volume-averaged kernels (Buffo *et al.*, 2016), which has been validated in closed stirred-tank (Castellano *et al.*, 2018), are implemented in the model to better account for the turbulence inhomogeneities in the 1D hydrodynamic model:

$$\bar{\Gamma}(v)=\frac{1}{V}\int_{V}\Gamma(v,\boldsymbol{x})\mathrm{d}\boldsymbol{x}=\int_{0}^{\infty}\Gamma(v,\varepsilon)f(\varepsilon)\mathrm{d}\varepsilon \qquad (4)$$

$$\bar{Q}(v,v')=\frac{1}{V}\int_{V}Q(v,v',\boldsymbol{x})\mathrm{d}\boldsymbol{x}=\int_{0}^{\infty}Q(v,v',\varepsilon)f(\varepsilon)\mathrm{d}\varepsilon \qquad (5)$$

In Eq. (4) and (5), $f(\varepsilon)$ represents the probability density function (PDF) of the turbulent kinetic energy dissipation rate ε, which defines the influence of the turbulent eddies in the droplet breakage and coalescence. $f(\varepsilon)$ can be obtained by CFD simulations of the liquid-liquid extractor. The final 1D PBE model reads:

$$\frac{\partial}{\partial t}n(v,z,t) + u_d(v,z,t)\frac{\partial}{\partial z}n(v,z,t)$$
$$= \int_v^\infty \beta(v|v')n(v',z,t)\int_0^\infty \Gamma(v,\varepsilon)f(\varepsilon)\mathrm{d}\varepsilon\,\mathrm{d}v'$$
$$- n(v,z,t)\int_0^\infty \Gamma(v,\varepsilon)f(\varepsilon)\mathrm{d}\varepsilon \tag{6}$$
$$+ \frac{1}{2}\int_0^v n(v-v',z,t)n(v',z,t)\int_0^\infty Q(v,v',\varepsilon)f(\varepsilon)\mathrm{d}\varepsilon\,\mathrm{d}v'$$
$$- n(v,z,t)\int_0^\infty n(v',z,t)\int_0^\infty Q(v,v',\varepsilon)f(\varepsilon)\mathrm{d}\varepsilon\,\mathrm{d}v'$$

The dispersed phase volume fraction $\phi(z,t)$ at a given location *z* and time *t* can be computed from the solution of the 1D PBE model:

$$\phi(z,t) = \int_{v_{\min}}^{v_{\max}} n(v',z,t)v'\,\mathrm{d}v' \tag{7}$$

2.1.1 Mass conservation

At each location in the axial domain, the PBE model requires the calculation of the velocity $u_d(v,z,t)$, as indicated in equation 6. The velocity of the dispersed phase can be obtained from that of the continuous phase, whichis determined by mass conservation in the column as well as the holdup obtained from the PBE. So, the PBE is coupled with the mass conservation model. The model assumes steady-state in the column (constant total flow rate of each phase). Consistently with this assumption, the mass flow rate of the continuous phase is uniform along the column $Q_\mathrm{c} = Q_\mathrm{c}^\mathrm{in}$. Hence, the superficial velocity $\mathrm{v_c}$ of the continuous phase reads:

$$\mathrm{v_c} = \frac{Q_\mathrm{c}^\mathrm{in}}{\Omega} = \big(1-\phi(z,t)\big)u_\mathrm{c}(z,t) \tag{8}$$

where Ω is the column section, and ϕ the holdup of the dispersed phase defined in Eq. (7). The relation between v_c and u_c, the real (or interstitial) velocity of the fluid, has been reminded as u_c is the velocity used in the slip velocity of the droplets introduced later in Eq. (9).

2.1.2 Hydrodynamics closure models

Coupling of the PBE with the 1D counter-current flow model requires the knowledge of the velocity for each class of droplet, $u_d(v,z,t)$, which depends on the droplet size. The velocity of a droplet class is defined with respect to the continuous phase velocity, introducing the relative (or slip) velocity $u_r(v,z,t)$, we have by definition:

$$u_d(v,z,t) = u_r(v,z,t) + u_c(z,t) \tag{9}$$

As in sedimentation problems (Richardson and Zaki, 1997), it is convenient to express the slip velocity as a function the equilibrium, or *terminal*, velocity of the droplet in the swarm, $U_\infty^\phi(d)$, which depends on the drop size, the terminal velocity of the same droplet alone, $U_\infty(d)$, and on the holdup, ϕ, which here depends on time and the axial location. In order to account for the effect of the packing and of the oscillation flow prevailing in the pulsed column ($U_\infty(d)$ being related to infinite media and quiescent fluid), an additional slowing factor, k_s, is introduced (Al Khani, Gourdon and Casamatta, 1989):

$$u_r(d,z,t) = k_s\, U_\infty^\phi(d) = k_s\, U_\infty(d)(1-\phi(z,t))^n \tag{10}$$

In the current version of *ColHySE*, the Schiller and Nauman model (L. Schiller Z. Naumann, 1935) is used to compute the drag coefficient C_d and from then the terminal velocity $U_\infty(d)$.

$$C_d = \frac{24}{Re_d}\left(1 + 0.15 Re_d^{0.687}\right), \qquad Re_d < 800 \tag{11}$$

with Re_d he droplet's Reynolds number.

The swarm coefficient, *n*, is always greater than 1 and is a function of the flow regime and of the relative diameter of the droplet and the column (Richardson and Zaki, 1997).

At last, a typical correlation for pulsed column (Gourdon and Casamatta, 1991) is used for the slowing factor k_s:

$$\begin{cases} k_s = 1 & \text{if } \frac{A}{H} \ll 1 \\ k_s = 0.5 & \text{if } \frac{A}{H} \approx 1 \end{cases} \quad (12)$$

Where H is the spacing between the packing elements and A the pulsation amplitude. According to this model, slowing is effective only when A and H are similar.

2.1.3 PBE closure models: breakage and coalescence

The source terms are based on the (Coulaloglou and Tavlarides, 1977) models for breakage and coalescence:

$$\Gamma(d) = C_1 \varepsilon^{1/3} d^{-2/3} \exp\left(-\frac{C_2 \gamma}{\rho_d \varepsilon^{2/3} d^{5/3}}\right) \quad (13)$$

$$Q(d,d') = C_3 (d^2 + d'^2)\left(d^{\frac{2}{3}} + d'^{\frac{2}{3}}\right)^{1/2} \varepsilon^{1/3} \exp\left(-\frac{C_4 \rho_c \mu_c \varepsilon}{\gamma^2}\left(\frac{dd'}{d+d'}\right)^4\right) \quad (14)$$

Where ρ_c and ρ_d are the densities of the continuous and dispersed phases, μ_c the viscosity of the continuous phase, and γ the surface tension. C_1, C_2, C_3 and C_4 are the model fitting parameters, that depend on the chosen hydrodynamic description, i.e. either the use of Eq. (13) and (14) with the mean dissipation rate in the column compartment, or of averaged as defined in Eq. (4) and (5).

2.1.4 Resolution of the PBE along the 1D axial domain

The Fixed Pivot Technique (FPT) is used to discretize the PBE (Kumar and Ramkrishna, 1996). This well-known sectional method is indeed robust, able to directly conserve the number (or volume) density function, and it is relatively easy to implement. The FTP is based on the discretization of the internal coordinate domain (here the droplet volume, v) in N_P intervals $[v_i, v_{i+1}]$ on which the 1D PBE model is integrated as follows:

$$\int_{v_i}^{v_{i+1}} \frac{\partial}{\partial t} n(z,v,t)\,\mathrm{d}v + \int_{v_i}^{v_{i+1}} u(z,v,t)\frac{\partial}{\partial z} n(z,v,t)\,\mathrm{d}v = \int_{v_i}^{v_{i+1}} S(z,v,t)\,\mathrm{d}v \qquad (15)$$

which leads to the following set of equations:

$$\frac{\partial}{\partial t} N_i(z,t) + \bar{u}(z,t)\frac{\partial}{\partial z} N_i(z,t) = S_i(z,t) \qquad (16)$$

where $N_i(z,t)$ represents the number of droplets which have dimensions in the i^{th} interval $[v_i, v_{i+1}]$, $\bar{u}(z,t)$ is the velocity of a droplet with volume $\frac{v_i + v_{i+1}}{2}$ computed according to Eq. (9) and $S_i(z,t)$ is the source term due to breakage and coalescence events that becomes:

$$\begin{aligned} S_i(z,t) \;=\; & \sum_{\substack{j,k \\ p_{i-1} \le (p_j + p_k) \le p_{i+1}}}^{j \ge k} \left(1 - \frac{1}{2}\delta_{j,k}\right) \eta\, Q_{j,k} N_j(z,t) N_k(z,t) - \Gamma_i N_i(z,t) \\ & - N_i(z,t) \sum_{k=1}^{M} Q_{i,k} N_k(z,t) + \sum_{k=1}^{M} m_{i,k}\, \Gamma_k N_k(z,t) \end{aligned} \qquad (17a)$$

where:

$$\eta \;= \begin{cases} \dfrac{p_{i+1} - v}{p_{i+1} - p_i} & p_i \le v \le p_{i+1} \\ \dfrac{v - p_{i-1}}{p_i - p_{i-1}} & p_{i-1} \le v \le p_i \end{cases} \qquad (17b)$$

and:

$$m_{ik} \;= \int_{x_i}^{x_{i+1}} \frac{p_{i+1} - v}{p_{i+1} - p_i} \beta(v, p_k) dv + \int_{x_{i-1}}^{x_i} \frac{v - p_{i-1}}{p_i - p_{i-1}} \beta(v, p_k) dv \qquad (17c)$$

The set of partial differential equations (16) is solved using a finite difference method, explicit in time. The accumulation term is discretized according to a first order approximation:

$$\frac{\partial N_i(z,t)}{\partial t} = \frac{N_{i,m}^{l+1} - N_{i,m}^{l}}{\Delta t} \qquad (18)$$

where the suffix *l* indicates the l^{th} step in time and the suffix *m* the m^{th} step in space.

Due to the hyperbolic nature of Eq. (16), a first order upwind scheme is implemented in the space discretization for stability purpose. Since the velocity of the i^{th} class of droplets can be either negative or positive (indeed, depending on their size, the droplets can either flow counter-currently or be conveyed by the continuous flow), two different approximations have been implemented:

$$\begin{aligned} &\bar{u}_i < 0 && \bar{u}_i \frac{\partial N_i(z,t)}{\partial z} = \bar{u}_i \frac{N_{i,m+1}^l - N_{i,m}^l}{\Delta z} \\ &\bar{u}_i > 0 && \bar{u}_i \frac{\partial N_i(z,t)}{\partial z} = \bar{u}_i \frac{N_{i,m}^l - N_{i,m-1}^l}{\Delta z} \end{aligned} \tag{19}$$

Finally, the $N_{i,m}^{l+1}$ can be computed as:

$$\begin{aligned} &\bar{u}_i < 0 && N_{i,m}^{l+1} = N_{i,m}^l - \bar{u}_i \frac{\Delta t}{\Delta z}(N_{i,m+1}^l - N_{i,m}^l) + \Delta t S_i \\ &\bar{u}_i > 0 && N_{i,m}^{l+1} = N_{i,m}^l - \bar{u}_i \frac{\Delta t}{\Delta z}(N_{i,m}^l - N_{i,m-1}^l) + \Delta t S_i \end{aligned} \tag{20}$$

2.2.5 Initial and boundary conditions of the axial domain

In most technical applications, the column is fed at the top by the liquid phase with the higher density, and at the bottom with the lower density phase, regardless of which of the two liquid is the dispersed one.

Regarding the continuous phase, the inlet flux is defined through the inlet superficial velocity v_c, as defined in Eq. (8).

At the initial time, the column is assumed to be filled only by the continuous phase. This gives the following distribution of droplets:

$$n(v, z, t = 0) = 0 \qquad \forall\, v, z \tag{21}$$

The size of the droplet at the inlet, d_{in}, is estimated according to the Scheele and Meister correlation (Mori and Mochizuki, 1992), giving the critical size of droplets at an orifice of diameter D_{in}:

$$\frac{\pi d_{\mathrm{in}}^3}{6} = F\left[\frac{\pi\gamma D_{\mathrm{in}}}{g\Delta\rho} + \frac{20\mu_{\mathrm{d}}Q_{\mathrm{d}}D_{\mathrm{in}}}{d_{\mathrm{in}}g\Delta\rho} - \frac{16\rho_{\mathrm{d}}{Q_{\mathrm{d}}}^2}{3\pi D_{\mathrm{in}}^2 g\Delta\rho} + \left(\frac{{Q_{\mathrm{d}}}^2 D_{\mathrm{in}}^2\rho_{\mathrm{d}}\gamma}{(g\Delta\rho)^2}\right)^{\frac{1}{3}}\right] \tag{22}$$

where F is the Harkins-Brown correction factor, given in (Mori and Mochizuki, 1992)

Alternately, if the column is equipped with a distributor, polydispersity of the droplets population can be assumed at the inlet, hence readings for the source term of Eq. (16) (Kronberger *et al.*, 1995):

$$S^{in}(t) = \frac{Q_{\mathrm{d}}}{\Omega}p^{\mathrm{in}}(v) \tag{23}$$

where $p^{\mathrm{in}}(v)$ is the droplet size distribution achieved by the distributor.

The column active length, L, is discretized in N_{L} parts of fixed size $\Delta z = \frac{L}{N_{\mathrm{L}}}$. The time step is adjusted in order to respect the Courant-Friedrichs-Lewy (CFL) criterion in order to ensure the stability of the explicit numerical scheme:

$$\begin{aligned} \bar{u_\iota} < 0 \qquad & 0 < \bar{u_\iota}\frac{\Delta t}{\Delta z} < 1 \\ \bar{u_\iota} > 0 \qquad & -1 < \bar{u_\iota}\frac{\Delta t}{\Delta z} < 0 \end{aligned} \tag{24}$$

Since the droplet velocity increases with its volume, the axial grid and the time-step are based on the upper limit of the droplet size range in which the PBE is resolved, and given by Eq. (22) or (23).

The advanced hydrodynamic model *ColHySE* has been programmed in Matlab®, to facilitate its use by chemical engineers concerned with solvent extraction column operation and/or designing. *ColHySE* computes the time-evolution of the DSD and the concentration of droplets (holdup), in each cell, all along the column axis. For the 25mm-ID column considered in the present case-study, the calculation time to reach stationary regime in the column varies between less than 1 minute and less than 5 minutes, when ran on an Intel Xeon dual-core machine (3.20 GHz) with 64GB of RAM, depending on whether uniform ε is assumed or not. The PBE and 1D axial mesh sizes were fixed to $N_{\mathrm{P}} = N_{\mathrm{L}} = 50$ following a preliminary mesh convergence study.

2.2 Case-study: The 25mm-ID disc-and-doughnut pulsed column

2.2.1 *Experiments*

The water-in-oil (Hydrogenated Tetra Propylene, TPH) flow in the 25mm-ID pulsed column has been studied by (Amokrane *et al.*, 2016). The column active height is L = 2 m. The distance between two successive packing elements, of thickness 1 mm, is equal to H = 24 mm. An air compressor, connected to the bottom settler through a pulsation leg, provides a sinusoidal oscillating motion of frequency F (imposed) and amplitude A. These oscillations promote the formation of a dispersion inside the column. For the sake of simplification, only the dispersed phase was flowing in most of the experiments ($Q_c = 0$), which flow rate Q_d was regulated to the chosen value by a syringe pump.

The droplet size distribution was monitored thanks to a SOPAT® endoscopic probe, inserted perpendicularly in the middle of the column (z = L/2), and positioned as closed as possible to the column wall, in order to reduce the flow perturbation. The DSD, and hence the Sauter mean diameter, were deduced by image processing. On the other hand, the dispersed phase volume fraction ϕ was determined by sampling small volumes of emulsion from the middle part of the column. The collected samples were centrifuged for 5 minutes at 5000 rpm, in order to separate the two phases before reading their respective volumes.

Experiments have been carried out at different dispersed phase flow rates and for pulsation intensities of AF = 20, 40 and 60 mm/s.

The mean drop diameter was observed to be a decreasing function of both the AF and Q_d. On the other hand, the holdup increased with Q_d and AF.

2.2.2 CFD simulations

In our previous study (Amokrane *et al.*, 2016), coupled CFD-PBE simulations were used to fit the Ci parameters, by an optimization procedure consisting of minimizing the error between the experimental and the simulation results (of the Sauter mean diameter and

holdup). The achieved methodology thus involved the computation of the local and instantaneous breakage and coalescence rates in the whole computational domain. *ColHySE* is instead based on volume-averaged kernels, that kernels require the knowledge of the probability distribution function of the turbulent dissipation rate in the contactor for the given operating conditions. We used ANSYS Fluent 17.2 to determine $f(\varepsilon)$ from single-phase flow simulations for each value of amplitude A considered in the experimental study. The computation domain consisted in 3 disks and 3 doughnuts (*i.e.* 3 compartments), and it was composed of 48,500 quadrilateral cells. An axisymmetric boundary condition is applied at the column axis, along with no-slip wall boundary conditions for the column internals. An inlet velocity condition is considered at one side, where a user defined function (udf) is used to impose the pulsed velocity, whereas an outlet pressure condition is imposed at the other side. The full methodology and details of the CFD model have already been described in (Amokrane *et al.*, 2016) and are not worth repeating here. As no continuous phase was considered, only the oscillating part of the flow was considered in the udf. The CFD simulations took around 5 hours each on an Intel Xeon dual-core machine (3.20 GHz) with 64 GB of RAM.

As each compartment of the whole column is assumed to undergo similar flow conditions far from the column ends, the distribution of ε was extracted from the central compartment of the computational domain. The number of bins was fixed to $N_{f(\varepsilon)}$ =100 after a prior convergence study. This distribution was moreover time-averaged using the Data Sampling Function of ANSYS Fluent. The full period of the oscillation, *i.e.* $1/F$, was chosen for the time-averaging procedure. The validity of this assumption is discussed in the next section. The resulting $f(\varepsilon)$ are illustrated in Fig. 2.

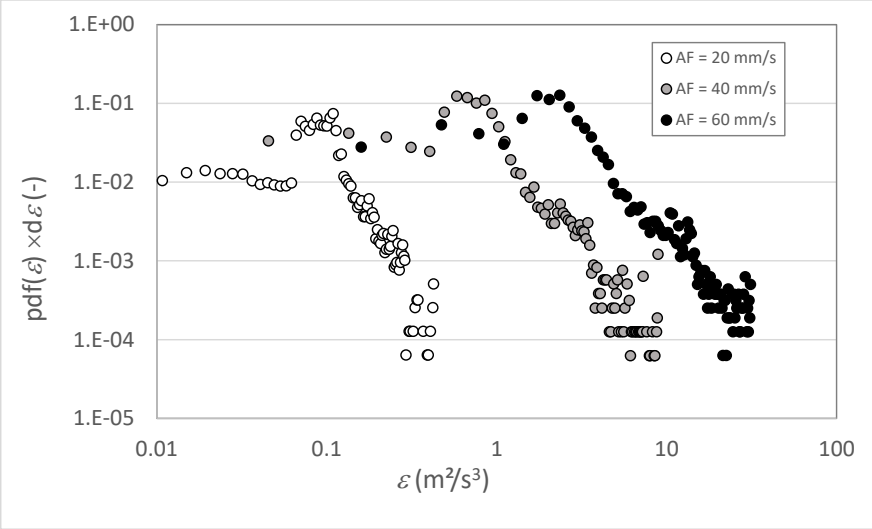

Figure 2: Time-averaged distribution of the function *f(ε)* of the energy dissipation in the middle compartment of the column obtained by CFD simulation. Effect of the pulsation intensity at F = 1 Hz.

The probability distribution functions were stored in the *ColHySE's* database (see Figure 1) under the form of a distribution function, defined as: $f(\varepsilon) = pdf(\varepsilon) \times d\varepsilon$, where $d\varepsilon$ is the width of the turbulence dissipation rate interval (or bin) used to construct the pdf. This is mandatory to convert the dimensionless pdf to the appropriate units (s^3/m^2) for kernel's integration purpose.

2.2.3 Adjustment of the kernels parameters and discussion

We selected the DSD measured at *AF* = 40 mm/s to adjust the averaged breakage and coalescence kernels parameters based on the Coulaloglou and Tavlarides framework. The identification procedure consisted in matching the experimental values of (Amokrane *et al.*, 2016) with the *ColHySE* numerical predictions of the holdup and mean droplets diameter, at steady-state in the central part of the column. Two sets of C_i parameters have been identified:

- A first set based on the original formulation of the kernels (or "uniform" kernels), achieving a double integration, in time and in the compartment's volume, of the turbulent dissipation rate, $\bar{\varepsilon}$;
- A second set based on the "averaged" kernels, considering the time-average of the turbulent dissipation rate distribution function, *f(ε)*, in the compartment.

The two sets of C_i are reported in Table 1.

Table 1: Parameters of the Coulaloglou and Tavlarides model for the pulsed column, assuming uniform dissipation and average kernels (this work), and values recommended by Amokrane for the same experiments, but based on coupled CFD-PBE simulations (Amokrane *et al.*, 2016). The values initially proposed by (Coulaloglou and Tavlarides, 1977) for liquid-liquid dispersions in stirred-tank is also reminded

	C_1	C_2	C_3	C_4
Uniform kernels based on $\bar{\varepsilon}$ – this work	$1.00\ 10^{-3}$	$6.35\ 10^{-2}$	$1.2\ 10^{-1}$	$1.33\ 10^{11}$
Averaged kernels based on pdf(ε) – this work	$2.30\ 10^{-2}$	$4.20\ 10^{-1}$	$2.30\ 10^{-2}$	$1.33\ 10^{11}$
(Amokrane *et al.*, 2016)	$8.03\ 10^{-2}$	$6.35\ 10^{-2}$	$4.50\ 10^{-2}$	$1.89\ 10^{11}$
(Coulaloglou and Tavlarides, 1977)	$4.78\ 10^{-3}$	$5.52\ 10^{-2}$	$2.17\ 10^{-4}$	$2.28\ 10^{13}$

As can be observed, changing the hydrodynamic description of the pulsed flow results in important changes in the values of the parameters used in the breakage (C_1 and C_2) and coalescence (C_3 and C_4) rates that best fit the experimental results.

In the Coulaloglou and Tavlarides model Eq. (13) and (14), the C_1 and C_3 parameters are used in the calculation of the energy of the interacting eddies in the breakage kernel (C_1), and of the droplets collisions frequency due to turbulent fluctuations in the coalescence kernel (C_3), both proportional to $\varepsilon^{1/3}$. It is therefore not surprising that C_1 and C_3 appear to be the most sensitive to the hydrodynamic description, compare to C_2 and C_4, respectively involved in the breakage probability and coalescence efficiency terms, also depending on ε, but through exponential negative terms that could only vary between 0 and 1.

3 Verification of the relevance and robustness of the model

Although the hydrodynamic description of the column is refined in *ColHySE* compared to previous 1D-PBE models, it still relies on models to describe the interactions between the two phases. These models, including Eq. (10)-(14) and (23), and the $f(\varepsilon)$ itself, are either empirical, involving experimentally adjusted parameters, or based on simplifying assumptions. A proper validation would require additional instrumented tests in pulsed column (monitoring of the DSD and holdup at different locations along the column, for

different fluids and operating conditions, ideally different packings and column geometries) and will be the scope of a future paper.

In this section, specific design of experiments was achieved in order to investigate the sensitivity of the *ColHySE* predictions to:

- the time averaging procedure used for the periodic flow encountered in pulsed column;
- the parameters of the closure equations Eq. (10)-(14) and (23).

3.1 Sensitivity to the time-averaging procedure

In the closed stirred-tank considered in (Castellano *et al.*, 2018), the residence time of the emulsion is large (considered infinite) and the mobile rotation frequency is high. The flow-field in the vessel was assumed time-independent, and hence was the probability distribution function of energy dissipation in the fluid volume, $pdf(\varepsilon)$. However, in lab-scale pulsed columns and with the typical operating conditions considered in Sec. 2, the residence time of the droplet is of the order of few minutes, whereas the global dynamic of the flow field is imposed by the period of the pulsation (typically 1 second). During each cycle, the local turbulence dissipation rate exhibits drastic changes, as evidenced by both PIV and CFD (Amokrane *et al.*, 2014). The characteristic time of the oscillation is therefore comparable to the droplets residence time in the compartment, which constitutes a major difference with the closed stirred-tank.

In *ColHySE*, as in other solvent extraction column simulators, the time-scale of the simplified 1D-axial problem is decoupled from the intrinsic dynamics of the flow. It is therefore important to study the effect of the size of the time-interval set of the average probability distribution function of ε (that will be used at each time step to calculate the average kernels), on the final results in terms of DSD and holdup profile in the column. In this aim, two different methodologies have been considered to derive $f(\varepsilon)$ from the single

phase CFD simulation (see Fig. 3) and the corresponding impact on the *ColHySE* predictions was studied.

- *Method 1*: The kernels are computed with the $f(\varepsilon)$ averaged over the whole pulsation period T. They are kept the same during the whole transient 1D-PBE simulation;
- *Method 2*: The kernels are computed with 10 different $f(\varepsilon)$, averaged over 10 successive time-intervals, $T_i = T/10$, to cover the full period. This means that the kernels have to be updated after each time-interval of the flow, hence imposing the code to compute periodically the time-averaged kernels, which significantly increases the simulation time (from minutes to hours).

The procedure was repeated for the 3 sets of operating conditions considered in Sec. 2, *e.g.* for a pulsation intensity of respectively 20, 40 and 60 mm/s.

The pd$f(\varepsilon)$ and breakage rates obtained by the two methods are compared in Fig. 3. for the case AF = 20 mm/s. The corresponding contours of epsilon are given in the SI. They provide information on where high and low turbulent dissipation rates are located in the compartment, and how they evolve along the period. For both cases, a non-negligible range of variation around the period-average value is highlighted. Also not shown, similar behaviours were observed at 40 and 60 mm/s, but with the pdf shifted to the right as AF increases (as illustrated in Fig. 2) while the breakage rate increases. The aim of this section is to evaluate the possible impact of these transient variations on the prediction of the steady-state DSD and holdup profile in the pulsed column.

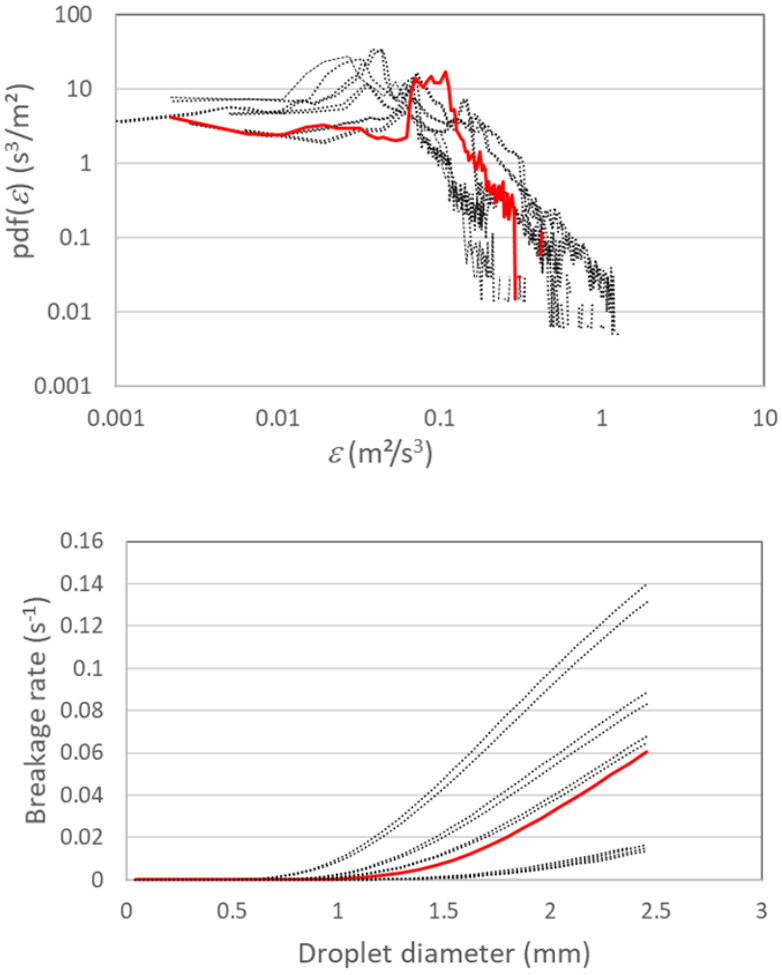

Figure 3: On the top: comparison of the period-averaged ε distributions, pdf(ε), from Method 1 (red plain lines), with the 10 interval-average distributions from Method 2 (black dot lines) for a pulsation intensity of 20 mm/s. On the bottom: comparison of the corresponding breakage rates computed by ColHySE. The time-intervals corresponding to the 10 dotted lines of Method 2 are skipped to avoid unnecessarily overloading the figures.

In order to avoid a fastidious optimization procedure, and as the aim of the study is to compare averaging procedures, not to achieve the best comparison between experiments and simulation, the same C_i parameters have been considered in both methods for the coalescence and breakage rates. We used the 2nd set of parameters identified in Sec. 2.3 and reported in Table 1 for the computation of the averaged kernels, whether they are based on the "period-averaged" $f(\varepsilon)$, method 1, or on the "interval-averaged" ones, method 2.

The holdup and mean diameter profiles obtained at steady-state are compared in Fig. 4 for the three considered pulsation amplitudes respectively. The corresponding DSD in the middle compartment of the column are reported in SI for the sake of illustration.

In each case, a flat profile is predicted for the mean diameter. In general, regardless of the time-averaging method, the coupled model predicts a reduction of the droplet size with the increase of the pulsation intensity.

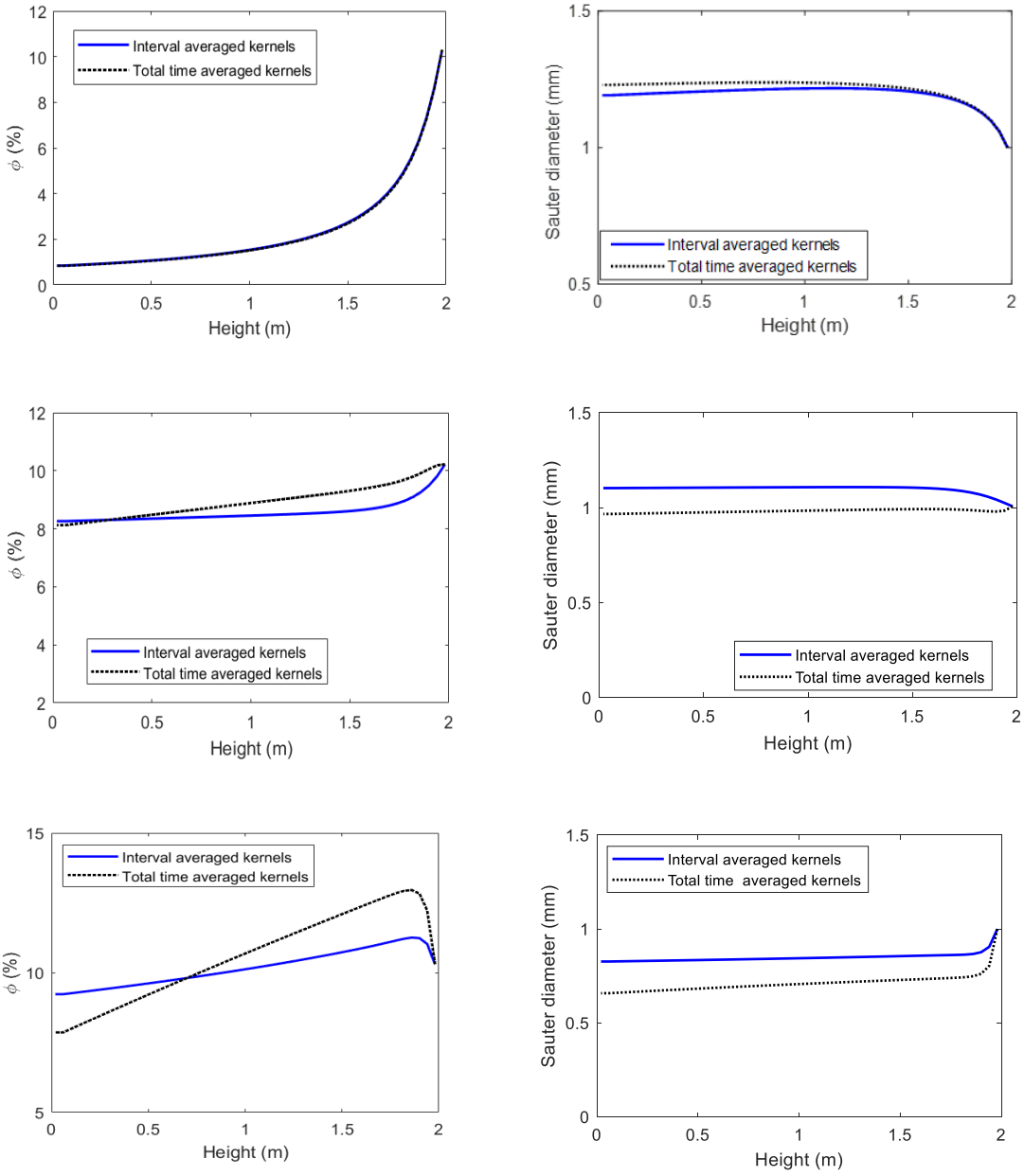

Figure 4: Impact of the time-averaging procedure on the profiles of the holdup (left) and the mean diameter (right) predicted by ColHySE along the column. Plain blue line: results obtained according to Method 1; dark dot line: results obtained following Method 2. The top, middle and bottom pictures are referring to AF = 20, 40, and 60 mm/s respectively. The inlet droplet diameter is 1 mm in each case. The DSD predicted by the model, at steady state, at the column center are given in SI.

Regarding the two proposed approaches, except for AF = 20 mm/s where the two methods give similar results, splitting the period into 10 time-intervals (method 2) results in smoother holdup profile and larger droplets, suggesting a different balance between breakage and coalescence rates between the two methods, with the period averaging method predicting smaller droplets. The deviation between the results predicted under method 1 and method 2 increases with the pulsation intensity. This deviation is negligible at 20 mm/s, and remains small at 40 mm/s. It is more pronounced at AF = 60 mm/s, especially regarding the holdup profile due to large fraction of tiny droplets predicted by method 1 (period-averaging). Compared to the corresponding experimental value at AF = 60 mm/s (d_{32} = 0.87 mm, see Tab. 2 in (Amokrane *et al.*, 2016)) , the algorithm with method 1 underestimates the mean diameter in the middle of the column by 18 %, which is still acceptable. The error drops to 3% using method 2. Although comparison with these experimental results is not a validation, due to the many other assumptions in the closure equations, this may suggest that splitting the period in the hydrodynamic description (method 2) may be more appropriated in configurations where the pulsation amplitude deviates strongly from the distance between the packing elements (here, A/H = 3 for AF = 60 mm/s). Since under typical operating conditions of discs-and-doughnuts pulsed column, the A/H ratio is generally below 1, and with regard to the simpler implementation of method 1 in ColHySE (also leading to significantly lower CPU requirements), the period-average kernel will be the preferred method for running *ColHySE* simulations in the following sections.

3.2 Sensitivity to the parameters of the closure models

Besides the numerical methods, for which parameters have been set thanks to classical "numerical convergence" studies, *ColHySE* mainly relies on three kinds of models:

- The breakage and coalescence models, Eq. (13) and (14). As previously mentioned, these models involve 4 adjusted parameters C_1, C_2, C_3, C_4, for which different sets of parameters are given in Table 1, depending on the hydrodynamic description used.
- The slip velocity model Eq. (10). The latter is the combination of the terminal velocity of a single droplet in quiescent liquid, that has no adjustable parameter, and of the Richardson and Zaki correction for swarm effect, which has 1 parameter, the swarm exponent n; and a slowing factor k_s to account for the combined effects of the packing and of the pulsation.
- The "advanced" hydrodynamic model is based on a distribution function that models the turbulent dissipation rate in the 3D domain. This pdf is deduced from single-phase RANS CFD simulations, meaning that the turbulence is assumed to be isotropic, among other assumptions, including the neglecting of particle induced turbulence, which is a strong assumption. In order to study the relative importance of the precision on the *pdf(ε)*, we will consider here that ε obeys a lognormal distribution which density probability function is based on 2 parameters: its mean μ and standard deviation σ, according to:

$$pdf(\varepsilon) = \frac{1}{\varepsilon\sigma\sqrt{2\pi}} \exp - \left(\frac{(\ln \varepsilon - \mu)^2}{2\sigma^2} \right) \tag{25}$$

The standard deviation and the mean were fitted on the period-averaged pdf deduced from the CFD simulations at 40 mm/s (see Sec. 2.2.2). The same procedure was repeated for the 10 interval-averaged pdf (see method 2 in Sec. 3.1), from which the ranges of variation of μ and σ were evaluated.

We studied the sensitivity of the holdup and d_{32} in the center point of the column (z = 1 m), under the same operating conditions as in Sec. 2.2.1 (water droplets in TPH, Q_c = 0, Q_d = 3.4 L/h, *AF*=40 mm/s), thanks to a e fractional factorial design of experiment (DOE). Fractional DOE are efficient tools to explore simultaneously the effects of different factors that are likely to influence the response of a system. The treatment consists of considering relevant combinations of these factors to screen their relative effects. With the chosen fractional factorial DOE, only 2-to-2 interactions are considered, the others being assumed negligible, which we consider sufficient as a first approximation.

The DOE considered 2 levels for each of the 8 parameters listed above and detailed in Table 2, resulting in a total of 32 simulations.

Table 2: Parameters of the DOE. The min and max levels are either preconized by the original authors (n, k_s, or corresponding to the variation range observed by CFD (μ, σ), or correspond to the min and max values of the parameters fitted by Amokrane, Castellano and this work based on pulsed column experiments (C_i)

Parameter's name	**Symbol**	**Index**	**Level -1**	**Level +1**
Slowing factor	k_s	x_1	0.5	1.0
Swarm exponent	n	x_2	2.40	4.65
Lognormal standard deviation of pdf(ε)	σ	x_3	0.6545	1.4476
Lognormal mean of pdf(ε)	μ	x_4	-2.1026	0.0143
Breakage parameter	C_1	x_5	$6.10\ 10^{-1}$	$8.03\ 10^{-2}$
Breakage parameter	C_2	x_6	$4.09\ 10^{-2}$	$4.20\ 10^{-1}$
Coalescence parameter	C_3	x_7	$2.30\ 10^{-2}$	$9.99\ 10^{2}$
Coalescence parameter	C_4	x_8	$1.33\ 10^{11}$	$5.23\ 10^{20}$

The general form of the response surface, including binary interactions, is given by the quadratic polynomial Eq. (26), where x_i stands for the DOE factors (Table 2). Although the results were quite scattered and revealed flooding (ϕ = 0) in some cases, we were able to identify the polynomial coefficients a_i and obtained a consistent statistical model for both the holdup and the Sauter mean diameter, in the form:

$$\hat{Y} = a_0 + \sum a_i x_i + \sum a_{ij} x_i x_j \qquad (26)$$

The interaction coefficients of Eq. (26) obtained for ϕ and for d_{32} are compared in SI. The holdup ϕ is mainly sensitive to the breakage parameters (C_1 being more influent than C_2) and to the parameters of the slip velocity model (n being more influent than k_s). These parameters are acting mainly in a coupled way. The coalescence parameters arrive in 3rd position, mainly in interaction with the breakage ones. At last, the coefficients associated with $f(\varepsilon)$ (in the lognormal formalism adopted here) arrives in 4th position, in interaction with either a breakage (for ϕ) or a coalescence (for μ) parameter.

On the other hand, d_{32} is equally sensitive to the breakage parameter C_1 and to coalescence parameters C_3 and C_4. Both coefficient have an equivalent but opposite effect, as increasing C_3 leads to an increase of the coagulation while increasing C_4 leads to a decrease of the coagulation efficiency (the same observation applies for the breakage parameters). As for the holdup, a substantial sensitivity toward the slip velocity model is revealed. Indeed, n and k_s are not only influent through coupling with the PBE parameters, but also individually. The interaction coefficients of n, and especially of k_s, were smaller for ϕ. At last, the impact of $f(\varepsilon)$ is less pronounced on the mean drop size than on the holdup.

This analysis made it possible to assess the relative influence of the various parameters of the 1D-PBE coupled model with respect to the two main results of the simulation:

- As ϕ and d_{32} are coupled, in particular through the slip velocity, the dependence on n and k_s is high for the 2 responses, thus reinforcing the need for further development of this hydrodynamic closure equation;
- The weak dependency on μ and σ reinforces the conclusion of Sec. 3.1 regarding the time-averaging procedure for $pdf(\varepsilon)$;
- At last, ϕ is much more sensitive to the breakage parameters C_1 and C_2 than to the coalescence ones. This may help designing specific experiments and properly

adjusting the respective weight of ϕ and d_{32} in the optimization procedure for future identification studies.

4 Application of *ColHySE* to the prediction of the hydrodynamic functioning of the pulsed column

In this last section, we intend to illustrate the potential of the advanced hydrodynamic model implemented in *ColHySE* to better predict the pulsed column performances following changes in their geometry and operating conditions. The same set of models parameters, considered nominal at this stage for a typical ID-25 mm DD column operated with non-viscous fluids (*e.g.* in the range of validity of the turbulent breakage and coalescence kernels implemented, see (Castellano *et al.*, 2019)), and given in Table 1 is conserved all over the study. However, here the Oil-in-Water configuration was chosen to illustrate that the model can handle both Water-in-Oil and Oil-in-Water configurations. The dispersed phase is assumed to enter the column as droplets which size follow a Normal Distribution law, with a mean value d_{in} and variance σ_{in}. Since the aim of this section is to sort the parameters with regard on how much they affect the d_{32} and the holdup, not to find precise quadratic models (or surface response), the kernels based on uniform turbulent energy dissipation are considered for the sake of simplicity. This moreover avoids to run (nearly) as many CFD simulation as experiments in the DOE However, the effect of the power input (AF) and of the internal geometry (T and H) on the average turbulent dissipation was considered, using the model proposed by (Milot *et al.*, 1990), with the power coefficient k evaluated following (Angelov and Gourdon, 2012), and implemented in most pulsed column simulators.

$$\bar{\varepsilon} = k(H,T) \times (AF)^3 \tag{27}$$

4.1 Sensitivity study to the operating conditions

The sensitivity of the holdup and the mean droplet size has been investigated using the design of experiments method, already implemented in Sec. 3.2, although here only geometrical and operating parameters are considered as the DOE factors. The fractional factorial DOE here considers 11 parameters, detailed in Table 3, resulting in a total of 64 simulations. In order to assess the impact of experimental and/or assembly uncertainty, on the column performances, the 2 levels considered were based on a +/- 10% variation around the nominal values for each factor. Although for most variables this "uncertainty" greatly exceeds the precision of physico-chemical and dimensional measurements, it enables (at least partly) to account for the evolutions likely to occur during the column operation, and due to *e.g.* thermal variation, mass transfer, pollution, or a slight displacement of the packing elements.

Table 3: Parameters of the "sensitivity study" DOE. The min and max levels correspond to a +/- 10% variation around the nominal values referred to as "Level 0"

Parameter's name	**Symbol**	**Index**	**Level 0**	**Level -1**	**Level +1**
Pulsation amplitude (mm)	A	x_1	20	18	22
Flow-rate, continuous phase (L/h)	Q_c	x_2	3.9	3.5	4.3
Flow-rate, dispersed phase (L/h)	Q_d	x_3	4.7	4.2	5.2
Density, continuous phase (kg/m^3)	ρ_c	x_4	998.2	898	1098
Viscosity, continuous phase (cPo)	μ_c	x_5	1.10	0.99	1.20
Density, dispersed phase (kg/m^3)	ρ_d	x_6	760.0	684	836
Surface tension (mN/m)	γ	x_7	43.0	38.7	47.3
Inlet mean diameter (mm)	d_{in}	x_8	1.0	0.9	1.1
Inlet variance of the DSD (mm)	σ_{in}	x_9	0.025	0.0225	0.0225
Free section (-)	T	x_{10}	0.23	0.207	0.253
Packing spacing (mm)	H	x_{11}	24.0	21.6	26.4

Regarding the values predicted for ϕ and d_{32} in the middle of the column, two response surfaces following the quadratic polynomial Eq. (25) have been established. The corresponding interaction coefficients are compared in SI.

Although it would be unreasonable to find physical meaning behind all the interaction parameters, it is clear that the parameters related to the residence time (or the slip velocity) of the droplet have a significant influence on the holdup:

- the pulsation intensity;
- the fluid densities, and their gradient through the combined coefficient a_{46};

- the continuous phase flow rate;
- the spacing between the packing elements.

As a matter of fact, these parameters have also a strong influence on the Sauter mean diameter. However, the droplet size is also sensitive to parameters affecting specifically the breakage and the coalescence rates, namely:

- the surface tension;
- and the free section of the packing, which is correlated for turbulent energy dissipation, similarly to the pulsation amplitude and the packing spacing.

These results are fully consistent with the real hydrodynamic behavior of the pulsed column, as observed experimentally over the years in hydrometallurgical processes, hence highlighting the relevance of the modelling approach adopted in *ColHySE*, and its potential to guide the design and optimization of pulsed columns.

4.2 Predicting stable column operation

In this section, all the parameters of the column and the closure models are fixed at their nominal values (see Table 3). We particularly investigate the evolution of the holdup with:

- the total specific flow rate, $(Q_c + Q_d)/\Omega$ (where Ω is the column cross sectional area), that represents the column capacity, and that is generally an invariant parameter in scale-up studies;
- the pulsation intensity AF;
- the ratio of the aqueous to the oil phase flow rate (typically named "A/O", here equal to Q_c/Q_d), which represents the slope of the operating line in the McCabe and Thiele diagram, and is hence related to the column efficiency with regard to the solvent requirements.

Compared to the previous section, the averaged kernels have been used, but assuming for the sake of simplification that $f(\varepsilon)$ is not affected by the continuous phase flow rate (only by AF).[*]

[*] Note that it has been shown by Castellano (Castellano, 2019) that the superposition of an axial velocity to the oscillating one leads to a higher turbulent intensity in the column.

It is observed that the retention first increases linearly with the flow rate. This growth slows down (at low pulsation intensity) or accelerates (at high pulsation intensity) as flooding is approached, which in the calculations is reflected by a sudden drop of the holdup to zero. In addition, the holdup values are higher when the A/O ratio is lower, and consequently flooding occurs earlier at lower Q_c/Q_d (or "A/O"). This behavior is consistent with experimental observations, where ϕ appears, in first approximation, a growing function of Q_d (here the oil phase flow-rate, O in "A/O") and a decreasing function of Q_c (here the aqueous phase flow-rate, A in "A/O) The resulting simulations are shown in Fig. 5 for the case $Q_c/Q_d = 1$.

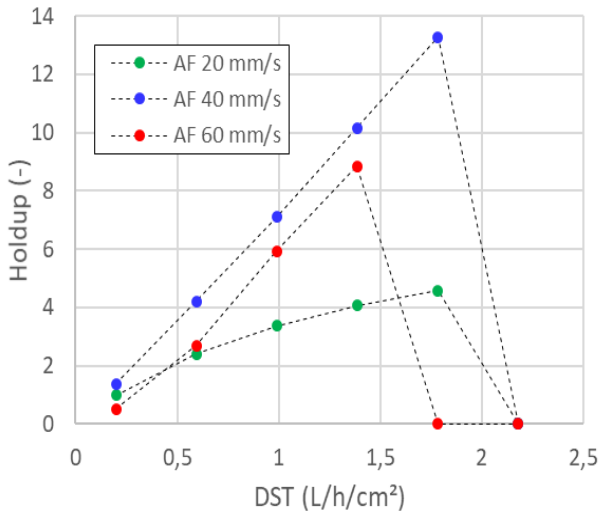

Figure 5: Evolution of the holdup in Oil-in-Water mode (TPH in Water) in the 25mm-ID pulsed column, in the case $Q_c/Q_d = 1$ (results for $Q_c/Q_d = 0.5$ and $Q_c/Q_d = 3.2$ are shown in SI).

The predicted effect of the pulsation intensity is less straightforward. Mostly, the ϕ values at 20 mm/s are lower than those calculated at 40 and 60 mm/s, which is consistent with the higher energy supplied to the system. Due to the axial component of the flow being neglected in the CFD simulations, it is neither possible nor relevant to draw any further conclusion about the effect of AF.

These preliminary results indicate however that the coupling of the PBE to represent the dispersed phase, with the advanced hydrodynamic description, is a sound methodology to assess the stability of the column.

5 Conclusion

The relevance of averaged-kernels to improve the droplet size distribution predicted in turbulent flow from the resolution of the PBE, while assuming a uniform contactor (0D-PBE problem) has been experimentally validated in closed agitated, *i.e.* with a constant holdup (Castellano *et al.*, 2018). This study demonstrated that the errors observed while using average kernels for different flow conditions, without systematic readjustment of the breakage and coalescence parameters, are considerably reduced compared to the use of kernels based on the mean turbulent dissipation. Indeed, these ones do not account for the possible flow heterogeneities. In this work, we have successfully transposed to the pulsed column.

In the continuous contactor problem, the PBE equation includes a convective term and is coupled to the uniform flow of the continuous phase. This implies additional closure terms, and parameters, compared to the closed contactor. Another and important difference relies on the “averaging” of the PBE source terms. In the case of the pulsed column, where the flow field varies periodically, the double-averaging is indeed required, for both space and time. At last, the volume fraction of the dispersed phase, or holdup ϕ, is not constant.

The relevance of the methodology, here based on the resolution of a 1D-PBE, was confirmed in the case of this continuous flow contactor, based on experimental data that were previously published (Amokrane *et al.*, 2016). Note that while the use of a 1D-PBE model to predict the properties of the dispersed phase in a liquid-liquid extraction column, has been recommended by many authors, starting with (Casamatta, 1981), in the model that we present, these predictions are made more robust to the modifications of the geometry of the

column (*i.e.* the spacing of the packing) of the column and of operating conditions (i.e. the pulsation parameters), because the “averaged” breakage and coalescence kernels used are able to properly account for the turbulent distribution in the column. This was made possible by the separate implementation of CFD simulations, the results of which, in terms of the turbulence distribution, can be stored as a simple text file in the database of the code. Thanks to this methodology, the new model proposed in this work is more suitable for sensitivity analysis and scale-up than those already used, as it can provide reasonably good trends in the evolution of the droplets size and concentration in the process, with affordable calculation times.

The relevance of the model's insight for solvent extraction processes was highlighted by two distinct sensitivity analysis. The sensitivity study of the new 1D-PBE approach to both the models parameters and the time-averaging procedure validated the robustness of the simulation results, as far as the flow patterns are not drastically changing. Additionally, the time-averaging of the coalescence and breakage kernels in oscillating flow (i.e. of the turbulent dissipation distribution function) was shown to have a minor effect for the typical operating conditions of the pilot-scale pulsed column used in R&D study. However, this point, specific to oscillating flow conditions, has to be further investigated for transposition to industrial columns, as well as the impact of the superimposed axial flow rate.

The parametric study in Sec. 3 confirms the strong interactions between the droplets size distribution (DSD) and the holdup, and highlights the major influence of the model used to calculate the slip velocity. Additional CFD simulations and dedicated experimental studies are therefore required in order to determine and to validate a sound set of parameters for two-phase flow closure models, and mainly the C_i, n and k_s.

Based on our current knowledge, we performed a sensitivity analysis of the dispersed phase properties to the column operating parameters. This additional DOE highlighted the great

flexibility of the proposed advanced hydrodynamic description for the prediction of the interfacial area, which is of prime importance for solvent extraction operations. The code capacity to predict the column flooding was moreover highlighted. The next step in the development of the code will be to couple the hydrodynamic description to the mass conservation of a chemical species that can be transferred between the two liquid phases.

Acknowledgment

Thus work was supported by the Energies Division of CEA (program SIACY). The authors gratefully acknowledge Lucia Sargentini from CEA/ISAS and Hervé Roussel from CEA/ISEC for the fruitful discussions and their advices on “best uncertainty analysis” and “best practice in pulsed column operation” respectively.

Nomenclature

CFD	Computational fluid dynamics
DD	Discs and doughnuts
DOE	Design of experiments
DSD	Droplets size distribution
ID	Internal diameter
FPT	Fixed pivot technique
PBE, PBM	Population balance equation, Population balance modelling
PIV	Particle imaging velocimetry
QMOM	Quadrature method of moments
RANS	Reynolds averaged Navier-Stokes equations
a_i	polynomial coefficients of the response surface Eq. (26)
A	Amplitude of the pulsation (m)
AF	Intensity of the pulsation (m/s)

C_i	Coefficients of the breakage (C_1 (m^{-2}), C_2) and coalescence (C_3, C_4) models
C_d	Drag coefficient
$pdf(\varepsilon)$	Probability density function of ε
d, d_{in}	Droplet's diameter, at the inlet (m)
d_{32}	Sauter mean diameter
D_{in}	Diameter of the orifice to generate the droplets in Eq. (22) (m)
F	Frequency of the pulsation (Hz)or Harkins-Brown coefficients in Eq. (22)
g	Gravity (m/s^2)
H	Spacing of the packing elements (m)
k_s	Slowing factor in Eq. (10)
L	Active length of the column (m)
n	Swarm coefficient in Eq. (10)
$n(v,z,t)$	Number density of droplet ($m^{-3}.m^{-3}$), variable of the PBE
$N_{f(\varepsilon)}$	Number of discretization intervals of the column
N_P	Number of discretization intervals of the $pdf(\varepsilon)$
N_L	Number of discretization intervals of the column
Q_{c} , $Q_{\mathrm{c}}^{\mathrm{in}}$	Mass flow rate of the continuous phase in the column, at the inlet (kg/s)
Q_{d}	Mass flow rate of the dispersed phase (kg/s)
Re_d	Droplet's Reynolds number
t	Time (s)
T	Period of pulsation (s), Free section of the column in Eq. (27)
v	Volume (internal coordinate of the PBE) (m^3)
u_c	Interstitial velocity of the continuous phase (m/s)
u_d	Velocity of a droplet class (m/s)
$U_\infty(d)$	Terminal velocity of an isolated droplet of size d (m/s)

$U_{\infty}^{\phi}(d)$	Terminal velocity of a droplet of size *d* in a swarm of holdup ϕ (m/s)
u_r	Relative (or slip) velocity of a droplet class(m/s)
v_c	Superficial velocity of the continuous phase (m/s)
x_i	Factors of the response surface Eq. (26)
z	Axial position in the column (m)
$\varepsilon, \overline{\varepsilon}$	Dissipation rate, average dissipation rate, of turbulent kinetic energy (m^2/s^3)
ϕ	Volume fraction of the dispersed phase (holdup)
γ	Surface tension (N/m)
μ	Lognormal mean of the *pdf(ε)*
μ_c, μ_d	Viscosity of the continuous, the dispersed phases (Pa.s)
ρ_c, ρ_d	Density of the continuous, the dispersed phases (km/m^3)
σ	Lognormal standard deviation of the *pdf(ε)*
Ω	Cross section of the column (m^2)

References

Alzyod, S., Attarakih, M. and Bart, H. J. (2018) 'CFD modelling of pulsed sieve plate liquid extraction columns using OPOSPM as a reduced population balance model: hydrodynamics and mass transfer', in *Computer Aided Chemical Engineering*. Elsevier B.V., pp. 451–456. doi: 10.1016/B978-0-444-64235-6.50081-4.

Amokrane, A. *et al.* (2014) 'Single-phase flow in a pulsed column: Particle Image Velocimetry validation of a CFD based model', *Chemical Engineering Science*, 114. doi: 10.1016/j.ces.2014.04.003.

Amokrane, A. *et al.* (2016) 'On droplets size distribution in a pulsed column. Part I: In-situ measurements and corresponding CFD-PBE simulations', *Chemical Engineering Journal*, 296. doi: 10.1016/j.cej.2016.03.089.

Angelov, G. and Gourdon, C. (2012) 'Pressure drop in pulsed extraction columns with internals of discs and doughnuts', *Chemical Engineering Research and Design*, 90(7), pp. 877–883. doi: 10.1016/j.cherd.2011.10.011.

Attarakih, M. *et al.* (2015) 'CFD-population balance modeling and simulation of coupled hydrodynamics and mass transfer in liquid extraction columns', *Applied Mathematical Modelling*, 39(17), pp. 5105–5120. doi: 10.1016/j.apm.2015.04.006.

Attarakih, M., Alzyod, S. and Fricke, A. (2017) 'Population balance modelling of pulsed packed bed extraction columns using PPBLab software', in *Computer Aided Chemical Engineering*. Elsevier B.V., pp. 67–72. doi: 10.1016/B978-0-444-63965-3.50013-1.

Batchelor, G. K. (1982) *The Theory of Homogeneous Turbulence*. New-York: ambridge University Press.

Boyadzhiev, L. and Spassov, M. (1982) 'On the size of drops in pulsed and vibrating plate extraction columns', *Chemical Engineering Science*, 37(2), pp. 337–340. doi: 10.1016/0009-2509(82)80169-3.

Buffo, A. *et al.* (2016) 'Simplified volume-averaged models for liquid–liquid dispersions: Correct derivation and comparison with other approaches', *Chemical Engineering Science*, 153, pp. 382–393. doi: 10.1016/j.ces.2016.07.032.

Casamatta, G. (1981) *Comportement de la population des gouttes dans une colonne d'extraction : transport, rupture, coalescence, transfert de matière.* Institut National Polytechnique de Toulouse.

Castellano, S. *et al.* (2018) 'Description of droplet coalescence and breakup in emulsions through a homogeneous population balance model', *Chemical Engineering Journal*, 354(July), pp. 1197–1207. doi: 10.1016/j.cej.2018.07.176.

Castellano, S. (2019) *Multiscale study and modeling of dispersion properties relevant for liquid-liquid extraction : adaptation of breakup and coalescence kernels to industrial processes*. Université Claude Bernard Lyon 1.

Castellano, S. *et al.* (2019) 'Using the full turbulence spectrum for describing droplet coalescence and breakage in industrial liquid-liquid systems: Experiments and modeling', *Chemical Engineering Journal*, 374, pp. 1420–1432. doi: 10.1016/j.cej.2019.06.032.

Coulaloglou, C. A. and Tavlarides, L. L. (1977) 'Description of interaction processes in agitated liquid-liquid dispersions', *Chemical Engineering Science*, 32(11), pp. 1289–1297. doi: 10.1016/0009-2509(77)85023-9.

Gourdon, C. and Casamatta, G. (1991) 'Influence of mass transfer direction on the operation of a pulsed sieve-plate pilot column', *Chemical Engineering Science*, 46(11), pp.

2799–2808. doi: 10.1016/0009-2509(91)85149-R.

Hlawitschka, M. W. *et al.* (2016) ‘CFD based extraction column design - Chances and challenges’, *Chinese Journal of Chemical Engineering*, 24(2), pp. 259–263. doi: 10.1016/j.cjche.2015.07.023.

J. C. Godfrey and Slater, M. J. (1994) *Liquid-liquid extraction equipment*. John Wiley. New-York.

Al Khani, S. D., Gourdon, C. and Casamatta, G. (1989) ‘Dynamic and steady-state simulation of hydrodynamics and mass transfer in liquid-liquid extraction column’, *Chemical Engineering Science*, 44(6), pp. 1295–1305. doi: 10.1016/0009-2509(89)85003-1.

Kronberger, T. *et al.* (1995) ‘Numerical simulation of extraction columns using a drop population model’, *Computers and Chemical Engineering*, 19(SUPPL. 1), pp. 639–644. doi: 10.1016/0098-1354(95)87107-1.

Kumar, A. and Hartland, S. (1996) ‘Unified Correlations for the Prediction of Drop Size in Liquid-Liquid Extraction Columns’, *Industrial & Engineering Chemistry Research*, 35(8), pp. 2682–2695. doi: https://doi.org/10.1021/ie950674w.

Kumar, S. and Ramkrishna, D. (1996) ‘On the solution of population balance equations by discretization - I. A fixed pivot technique’, *Chemical Engineering Science*, 51(8), pp. 1311–1332. doi: 10.1016/0009-2509(96)88489-2.

L. Schiller Z. Naumann (1935) ‘A Drag Coefficient Corre-lation’, *VDI Zeitung*, 77, pp. 318–320.

Li, D. *et al.* (2017) ‘Droplet breakage and coalescence in liquid–liquid dispersions: Comparison of different kernels with EQMOM and QMOM’, *AIChE Journal*, 63(6), pp. 2293–2311. doi: 10.1002/aic.15557.

Marchisio, D. L. and Fox, R. O. (2013) *Computational Models for Polydisperse Particulate and Multiphase Systems*. Cambridge: Cambridge University Press. doi: 10.1017/CBO9781139016599.

Marchisio, D. L., Vigil, R. D. and Fox, R. O. (2003) ‘Quadrature method of moments for aggregation-breakage processes’, *Journal of Colloid and Interface Science*, 258(2), pp. 322–334. doi: 10.1016/S0021-9797(02)00054-1.

Milot, J. F. *et al.* (1990) ‘Simulation of a pneumatically pulsed liquid-liquid extraction column’, *The Chemical Engineering Journal*, 45(2), pp. 111–122. doi: 10.1016/0300-9467(90)80033-9.

Mori, Y. H. and Mochizuki, T. (1992) ‘Explicit expressions for volume of drops released from submerged nozzles: their derivation from semiempirical implicit correlations’, *International Journal of Multiphase Flow*, 18(1), pp. 141–144. doi: 10.1016/0301-9322(92)90011-5.

Pacek, A. W., Man, C. C. and Nienow, A. W. (2005) *On the Sauter mean diameter and size distributions in turbulent liquid/liquid dispersions in a stirred vessel, Chemical Engineering Science*.

Ramkrishna, D. (2000) *Population balances: theory and applications to particulate systems in engineering*. Academic P. San Diego, CA.

Richardson, J. F. and Zaki, W. N. (1997) ‘Sedimentation and fluidisation: Part I’, *Chemical Engineering Research and Design*, 75(1 SUPPL.), pp. S82–S100. doi: 10.1016/s0263-8762(97)80006-8.